A Wideband Bandpass Power Divider With Out-of-Band Multi-Transmission Zeros and Controllable Equal-Ripple Levels

Nan Zhang, Xiaolong Wang, *Member, IEEE*, Lei Zhu, *Fellow, IEEE*, and Geyu Lu

***Abstract*— In this article, a novel wideband bandpass power divider (PD) with out-of-band multi-transmission zeros (TZs) is presented. It consists of $2M$ shunted short-circuited stubs (SCSs), $(M + N)$ cascaded coupled line sections, and $(M + N - K_N)$ isolation resistors. There are two types of topologies, and the number of TZs is solely determined by N. Through even- and odd-mode analyses, general simultaneous equations for characteristic impedances, coupling strengths, and isolation resistors are derived with the proposed algorithm. By suitably selecting all the design parameters, all the S-parameters (S_{11}, $S_{21} = S_{31}$, $S_{22} = S_{33}$, and S_{32}) of the proposed topology could provide an equal-ripple response with controllable ripple level in the passband. For a given fractional bandwidth (FBW), TZs and out-of-band rejection level can be designed independently. For further optimization, several isolation resistors can be omitted with the unchanged performances. For verification, two experimental circuits are fabricated and measured. Good agreement between the measured and simulated results is attained so as to successfully validate the correctness of the proposed design approach.**

***Index Terms*— Bandpass, equal-ripple, multi-transmission zero (TZ), power divider (PD), wideband.**

I. Introduction

POWER divider (PD) is a crucial microwave component and widely used in various wireless communication systems. Wilkinson PD (WPD) [1] is the most popular topology among various reported PDs, because it can not only split the power into two output ports but also achieve excellent port-to-port isolation performance and perfect impedance matching at all the ports at center frequency.

In RF front-end module, WPDs are usually cascaded with bandpass filters (BPFs) to cut off undesired signals. However, these discrete components need a large occupied area on the limited RF front-end circuit. By merging the WPD and BPF into single component, circuit size and transmission loss can be much smaller. Recently, filtering PDs become highlighted, and a variety of filtering PDs have been developed with different operation bandwidths. For bandpass PDs, there are two mainly filtering analysis approaches: classical admittance inverter approach [2]–[8] and coupling matrix network synthesis approach [9]–[15]. Other approaches may also be applied for PD design, for example, non-resonating nodes' approach [16].

To improve the operating bandwidth, a variety of wideband/ultra-wideband (UWB) bandpass (BP) PDs have been developed with different techniques. These techniques can be classified as microstrip-to-slotline technique [17]–[20], transversal signal-interference technique [21], ring resonator technique [22], coupled-line section (CLS), open-/short-circuited stub technique [23]–[31], and so on. Multi-way PDs with wideband filtering function [32]–[36] have also been reported, recently. Because multi-layer structure needs extra fabrication cost, microstrip-to-slotline technique is not highly preferred in industrial application. Additional transmission zeros (TZs) can be created outside the desired passband by transversal signal interference technique [21] and ring resonator technique [22], respectively. However, these ring-type topologies have to occupy a large circuit area.

Although equal-ripple response of S_{11} has been realized in different types of wideband topologies by using CLS and open-/short-circuited stubs (SCSs) [24], [29]–[31], the tasks in increasing the number of TZs with equal-ripple performance and suppressing out-of-band rejection level are still two big challenges. On the other hand, in-band reflection and isolation performances are two key design requirements in practice. In [30], a two-way PD is added to enhance the isolation performance and roughly maintain the operating bandwidth. However, the reflection performance (S_{22}) is not as good as isolation performance (S_{32}). By inserting multi-isolation resistors [29], [31], the numbers of reflection zeros (RZs) (RZs, where $S_{22} = S_{33} = 0$) at output ports and isolation zeros (IZs, where $S_{32} = 0$) between output ports are increased accordingly. But such kind of topologies cannot provide extra TZs. To sum up, no wideband BP PD topology has been developed so far to achieve the following performances: 1) designable multi-TZs and multi-RZs, controllable out-of-band rejection level, and wideband equal-ripple response of S_{11} and 2) controllable equal-ripple levels of reflection (S_{22}) and isolation (S_{32}) in the passband.

Manuscript received February 11, 2021; revised June 2, 2021 and September 17, 2021; accepted September 24, 2021. Date of publication October 7, 2021; date of current version February 7, 2022. This work was supported in part by the National Natural Science Foundation of China under Grant 61701189, Grant 61831011, and Grant 61833006; in part by the Project of the Education Department of Jilin Province under Grant JJKH20211093KJ; in part by the Project on Industrial Innovation Capability of Jilin Province under Gran 2020C048; in part by the Interdisciplinary Integration and Innovation Project of Jilin University (JLU) under Grant JLUXKJC2020204; and in part by "the Fundamental Research Funds for the Central Universities." *(Corresponding author: Xiaolong Wang.)*

Nan Zhang, Xiaolong Wang, and Geyu Lu are with the State Key Laboratory of Integrated Optoelectronics, College of Electronic Science and Engineering, Jilin University, Changchun 130012, China (e-mail: brucewang@jlu.edu.cn; smalld729@hotmail.com).

Lei Zhu is with the Department of Electrical and Computer Engineering, Faculty of Science and Technology, University of Macau, Macau, China.

Color versions of one or more figures in this article are available at https://doi.org/10.1109/TMTT.2021.3116072.

Digital Object Identifier 10.1109/TMTT.2021.3116072

In this article, a class of wideband BP PD is newly introduced. It consists of $2M$ shunted SCSs and $(M+N)$ cascaded CLSs, where $M \geq 2$ and $N \geq 2$. For even and odd numbers of N, there are two types of topologies, where the numbers of TZs ($S_{21} = 0$) and RZs ($S_{11} = 0$) are only determined by N and M, respectively. Through even- and odd-mode analyses, general simultaneous equations for characteristic impedances, coupling strengths, and isolation resistors are newly derived with the proposed algorithm. By suitably selecting all the design parameters, all the S-parameters (S_{11}, $S_{21} = S_{31}$, $S_{22} = S_{33}$, and S_{32}) of the proposed topology could provide controllable equal-ripple responses in the passband. Meanwhile, for a given fractional bandwidth (FBW), TZs and out-of-band rejection level can be designed independently. For further optimization, several isolation resistors can be omitted with the same performances to be maintained.

Compared with other reported works [17]–[36], the proposed topology could offer the following three unique features by virtue of the algorithm: 1) multi-TZs, multi-RZs, and out-of-band rejection level can be designed independently while maintaining equal-ripple response of S_{11}; 2) the numbers and frequencies of output port RZs ($S_{22} = S_{33} = 0$)/IZs ($S_{32} = 0$) can exactly match with those of input port RZs ($S_{11} = 0$), and both reflection and isolation ripple levels can be adjusted in the desired ranges in the passband; and 3) a unified design guideline with the proposed algorithm and optimization approach for isolation resistors are newly summarized and proved in this work.

II. Design Equations of Proposed Wideband BP PD

The topology of the proposed wideband BP PD is shown in Fig. 1. It consists of $2M$ shunted SCSs and $(M+N)$ cascaded CLSs, where $M \geq 2$ and $N \geq 2$. When N is an even integer, there are $(M+N)$ isolation resistors ($R_1, R_2, \ldots, R_{M+N}$); when N is an odd integer, there are $(M+N-1)$ isolation resistors ($R_1, R_2, \ldots, R_{M+N-1}$), where the position of the $(M+N)$th isolation resistor is replaced by via-hole so as to be connected with the ground. Z_{ei} and Z_{oi} are the even- and odd-mode characteristic impedances of the ith CLS (where $i = 1, 2, \ldots, M+N$). Z_{sj} is the characteristic impedance of the jth SCS (where $j = 1, 2, \ldots, M$). The electrical lengths of each CLS and SCS are set as θ. Three terminal load impedances are normalized to 1 Ω.

A. Even-Mode Analysis

Fig. 2(a) shows the even-mode equivalent bisection circuit of the proposed wideband BP PD. The input admittance Y_{sine} can be calculated as

$$Y_{\text{sine}} = jg_s \sin\theta \frac{\sum_0^{(N+K_N)/2-1} g_i^{\text{up}} \cos^{2i+1}\theta}{\sum_0^{(N+K_N)/2} g_i^{\text{down}} \cos^{2i}\theta} \tag{1}$$

where $K_N = \text{mod}(N, 2)$, and g_i^{up} and g_i^{down} are the polynomial functions with the degrees $(2i+1)$ and $2i$, respectively. g_s, g_i^{up}, and g_i^{down} are only determined by the even-mode characteristic impedances of N cascaded CLSs ($Z_{eM+1}, \ldots, Z_{eM+N}$).

The entire ABCD matrix of the even-mode equivalent bisection circuit in Fig. 2(a) can be derived by multiplying

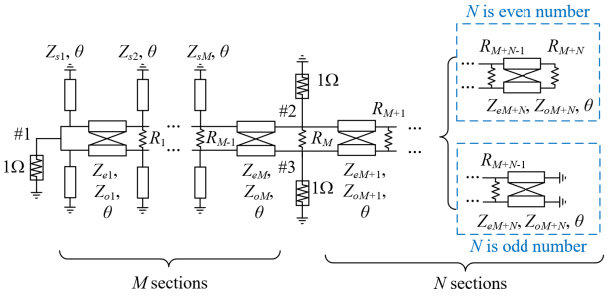

Fig. 1. Topology of the proposed wideband BP PD.

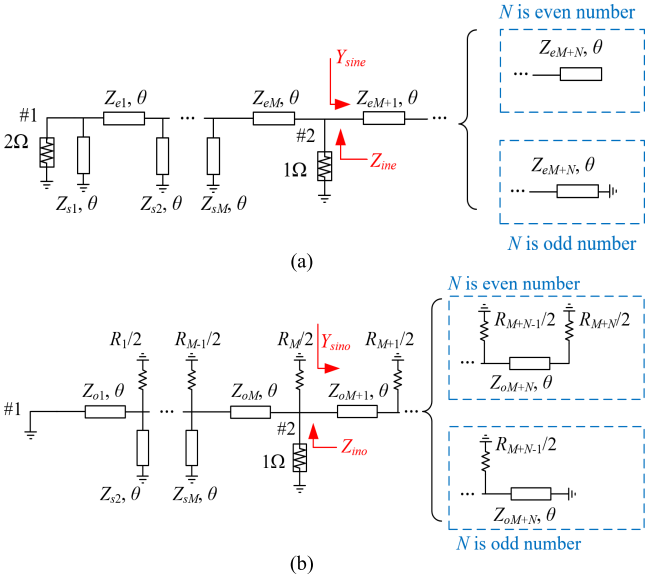

Fig. 2. Formulation of the even- and odd-mode equivalent bisection circuits for the proposed wideband BP PD. (a) Even-mode. (b) Odd-mode.

the ABCD matrices of cascaded sections, such that

$$\begin{bmatrix} A_e & B_e \\ C_e & D_e \end{bmatrix} = \begin{bmatrix} 1 & 0 \\ 1/(jZ_{s1}\tan\theta) & 1 \end{bmatrix} \begin{bmatrix} \cos\theta & jZ_{e1}\sin\theta \\ j\sin\theta/Z_{e1} & \cos\theta \end{bmatrix} \times \begin{bmatrix} 1 & 0 \\ 1/(jZ_{s2}\tan\theta) & 1 \end{bmatrix} \cdots \begin{bmatrix} 1 & 0 \\ 1/(jZ_{sM}\tan\theta) & 1 \end{bmatrix} \times \begin{bmatrix} \cos\theta & jZ_{eM}\sin\theta \\ j\sin\theta/Z_{eM} & \cos\theta \end{bmatrix} \begin{bmatrix} 1 & 0 \\ Y_{\text{sine}} & 1 \end{bmatrix}. \tag{2}$$

After complicated arithmetical operation, in (2) can be simplified as

$$A_e = \sum_0^{(M-K_M)/2} a_{\text{ei}} \cos^{2i+K_M}\theta - g_s \sum_0^{(M+K_M)/2} b_{\text{ei}} \cos^{2i+1-K_M}\theta \times \frac{\sum_0^{(N+K)/2-1} g_i^{\text{up}} \cos^{2i+1}\theta}{\sum_0^{(N+K)/2} g_i^{\text{down}} \cos^{2i}\theta} \tag{3a}$$

$$B_e = \frac{j}{\sin\theta} \sum_0^{(M+K_M)/2} b_{\text{ei}} \cos^{2i+1-K_M}\theta \tag{3b}$$

$$C_e = \frac{j}{\sin\theta} \sum_0^{(M+K_M)/2} c_{\text{ei}} \cos^{2i+1-K_M}\theta + jg_s \sin\theta \sum_0^{(M-K_M)/2} d_{\text{ei}} \times \cos^{2i+K_M}\theta \frac{\sum_0^{(N+K)/2-1} g_i^{\text{up}} \cos^{2i+1}\theta}{\sum_0^{(N+K)/2} g_i^{\text{down}} \cos^{2i}\theta} \tag{3c}$$

$$D_e = \sum_0^{(M-K_M)/2} d_{\text{ei}} \cos^{2i+K_M}\theta \tag{3d}$$

where $K_M = \mathrm{mod}(M, 2)$, a_{ei} and d_{ei} are the polynomial functions with the degree $(2i + K_M)$, and b_{ei} and c_{ei} are the polynomial functions with the degree $(2i + 1 - K_M)$.

a_{ei}, b_{ei}, c_{ei}, and d_{ei} are only determined by the even-mode characteristic impedances of M cascaded CLSs $(Z_{e1}, \ldots, Z_{eM})$ and the characteristic impedances of M shunted SCSs $(Z_{s1}, \ldots, Z_{sM})$. The input impedance Z_{ine} and reflection coefficient Γ_e looking into port 2 can be derived as

$$Z_{\mathrm{ine}} = (2D_e + B_e)/(2C_e + A_e) \quad \text{and} \quad \Gamma_e = (Z_{\mathrm{ine}} - 1)/(Z_{\mathrm{ine}} + 1). \tag{4}$$

Then, S_{11}, S_{21}, and S_{31} can be summarized as

$$S_{11} = \Gamma_e \quad \text{and} \quad S_{21} = S_{31} = 2\sqrt{2}/(A_e + B_e + 2C_e + 2D_e). \tag{5}$$

B. Odd-Mode Analysis

Similarly, Fig. 2(b) shows the odd-mode equivalent bisection circuit of the proposed wideband BP PD. The input admittance Y_{sino} can be calculated by

$$Y_{\mathrm{sino}} = \frac{\sum_0^N h_i^{\mathrm{up\_Re}} \cos^{2i}\theta + j\sin\theta \sum_0^{N-1} h_i^{\mathrm{up\_Im}} \cos^{2i+1}\theta}{\sum_0^N h_i^{\mathrm{down}} \cos^{2i}\theta} \tag{6}$$

where $h_i^{\mathrm{up\_Re}}$, h_i^{down}, and $h_i^{\mathrm{up\_Im}}$ are the polynomial functions with the degrees $2i$ and $(2i + 1)$, respectively. $h_i^{\mathrm{up\_Re}}$, h_i^{down}, and $h_i^{\mathrm{up\_Im}}$ are only determined by the odd-mode characteristic impedances of N cascaded CLSs $(Z_{oM+1}, \ldots, Z_{oM+N})$ and isolation resistors $(R_1, R_2, \ldots, R_{M+N})$.

The ABCD matrices of the odd-mode equivalent bisection circuit in Fig. 2(b) can be expressed as (7), shown at the bottom of the page.

After complicated arithmetical operation, (8) as shown at the bottom of the page, can be simplified, where $a_{\mathrm{oi}}^{\mathrm{Re}}$, $a_{\mathrm{oi}}^{\mathrm{Im}}$, $b_{\mathrm{oi}}^{\mathrm{Re}}$, $b_{\mathrm{oi}}^{\mathrm{Im}}$, $c_{\mathrm{oi}}^{\mathrm{Re}}$, $c_{\mathrm{oi}}^{\mathrm{Im}}$, $d_{\mathrm{oi}}^{\mathrm{Re}}$, and $d_{\mathrm{oi}}^{\mathrm{Im}}$ are the polynomial functions with the degree $(2i + K_M)$.

Similarly, $a_{\mathrm{oi}}^{\mathrm{Re}}$, $a_{\mathrm{oi}}^{\mathrm{Im}}$, $b_{\mathrm{oi}}^{\mathrm{Re}}$, $b_{\mathrm{oi}}^{\mathrm{Im}}$, $c_{\mathrm{oi}}^{\mathrm{Re}}$, $c_{\mathrm{oi}}^{\mathrm{Im}}$, $d_{\mathrm{oi}}^{\mathrm{Re}}$, and $d_{\mathrm{oi}}^{\mathrm{Im}}$ are only determined by the odd-mode characteristic impedances of M cascaded CLSs $(Z_{o1}, \ldots, Z_{oM})$, the characteristic impedances of M shunted SCSs $(Z_{s1}, \ldots, Z_{sM})$, and isolation resistors $(R_1, \ldots, R_M)$. Then, the input impedance Z_{ino} and reflection coefficient Γ_o looking into port 2 can be derived as

$$Z_{\mathrm{ino}} = B_o/A_o \quad \text{and} \quad \Gamma_o = (Z_{\mathrm{ino}} - 1)/(Z_{\mathrm{ino}} + 1). \tag{9}$$

Then, S_{22}, S_{33}, and S_{32} can in general be deduced as

$$S_{22} = S_{33} = (\Gamma_e + \Gamma_o)/2 \quad \text{and} \quad S_{32} = (\Gamma_e - \Gamma_o)/2. \tag{10}$$

III. Design Approach of Proposed Wideband BP PD

A. General Response of Proposed Wideband BP PD

A schematic of general S-parameters is shown in Fig. 3. In this work, the proposed wideband BP PD could not only

$$\begin{aligned}
&\begin{bmatrix} A_o & B_o \\ C_o & D_o \end{bmatrix} \\
&= \begin{bmatrix} 1 & 0 \\ 1/j(Z_{o1} + Z_{s2})\tan\theta + 2/R_1 & 1 \end{bmatrix} \cdots \begin{bmatrix} 1 & 0 \\ 1/jZ_{sM}\tan\theta + 2/R_{M-1} & 1 \end{bmatrix} \\
&\quad \times \begin{bmatrix} \cos\theta & jZ_{oM}\sin\theta \\ j\sin\theta/Z_{oM} & 1 \end{bmatrix} \begin{bmatrix} 1 & 0 \\ 2/R_{M+1} & 1 \end{bmatrix} \begin{bmatrix} 1 & 0 \\ Y_{\mathrm{sino}} & 1 \end{bmatrix}
\end{aligned} \tag{7}$$

$$\begin{aligned}
A_o = {} & \sum_0^{(M+K_M)/2-1} a_{\mathrm{oi}}^{\mathrm{Re}} \cos^{2i-K_M+1}\theta + \sum_0^{(M+K_M)/2-1} b_{\mathrm{oi}}^{\mathrm{Re}} \cos^{2i-K_M+1}\theta \frac{\sum_0^N h_i^{\mathrm{up_Re}} \cos^{2i}\theta}{\sum_0^N h_i^{\mathrm{down}} \cos^{2i}\theta} - \sum_0^{(M-K_M)/2} b_{\mathrm{oi}}^{\mathrm{Im}} \cos^{2i+K_M}\theta \\
& \times \frac{\sum_0^{N-1} h_i^{\mathrm{up_Im}} \cos^{2i+1}\theta}{\sum_0^N h_i^{\mathrm{down}} \cos^{2i}\theta} + j\left(\frac{1}{\sin\theta} \sum_0^{(M-K_M)/2} a_{\mathrm{oi}}^{\mathrm{Im}} \cos^{2i+K_M}\theta + \sum_0^{(M+K_M)/2-1} b_{\mathrm{oi}}^{\mathrm{Re}} \cos^{2i-K_M+1}\theta \frac{\sin\theta \sum_0^{N-1} h_i^{\mathrm{up_Im}} \cos^{2i+1}\theta}{\sum_0^N h_i^{\mathrm{down}} \cos^{2i}\theta} \right. \\
& \left. + \frac{1}{\sin\theta} \sum_0^{(M-K_M)/2} b_{\mathrm{oi}}^{\mathrm{Im}} \cos^{2i+K_M}\theta \frac{\sum_0^N h_i^{\mathrm{up_Re}} \cos^{2i}\theta}{\sum_0^N h_i^{\mathrm{down}} \cos^{2i}\theta} \right)
\end{aligned} \tag{8a}$$

$$B_o = \sum_0^{(M+K_M)/2-1} b_{\mathrm{oi}}^{\mathrm{Re}} \cos^{2i-K_M+1}\theta + \frac{j}{\sin\theta} \sum_0^{(M-K_M)/2} b_{\mathrm{oi}}^{\mathrm{Im}} \cos^{2i+K_M}\theta \tag{8b}$$

$$\begin{aligned}
C_o = {} & \sum_0^{(M+K_M)/2-1} c_{\mathrm{oi}}^{\mathrm{Re}} \cos^{2i-K_M+1}\theta + \sum_0^{(M+K_M)/2-1} d_{\mathrm{oi}}^{\mathrm{Re}} \cos^{2i-K_M+1}\theta \frac{\sum_0^N h_i^{\mathrm{up_Re}} \cos^{2i}\theta}{\sum_0^N h_i^{\mathrm{down}} \cos^{2i}\theta} - \sum_0^{(M-K_M)/2} d_{\mathrm{oi}}^{\mathrm{Im}} \cos^{2i+K_M}\theta \\
& \times \frac{\sum_0^{N-1} h_i^{\mathrm{up_Im}} \cos^{2i+1}\theta}{\sum_0^N h_i^{\mathrm{down}} \cos^{2i}\theta} + j\left(\frac{1}{\sin\theta} \sum_0^{(M-K_M)/2} c_{\mathrm{oi}}^{\mathrm{Im}} \cos^{2i+K_M}\theta + \sum_0^{(M+K_M)/2-1} d_{\mathrm{oi}}^{\mathrm{Re}} \cos^{2i-K_M+1}\theta \frac{\sin\theta \sum_0^{N-1} h_i^{\mathrm{up_Im}} \cos^{2i+1}\theta}{\sum_0^N h_i^{\mathrm{down}} \cos^{2i}\theta} \right. \\
& \left. + \frac{1}{\sin\theta} \sum_0^{(M-K_M)/2} d_{\mathrm{oi}}^{\mathrm{Im}} \cos^{2i+K_M}\theta \frac{\sum_0^N h_i^{\mathrm{up_Re}} \cos^{2i}\theta}{\sum_0^N h_i^{\mathrm{down}} \cos^{2i}\theta} \right)
\end{aligned} \tag{8c}$$

$$D_o = \sum_0^{(M+K_M)/2-1} d_{\mathrm{oi}}^{\mathrm{Re}} \cos^{2i-K_M+1}\theta + \frac{j}{\sin\theta} \sum_0^{(M-K_M)/2} d_{\mathrm{oi}}^{\mathrm{Im}} \cos^{2i+K_M}\theta \tag{8d}$$

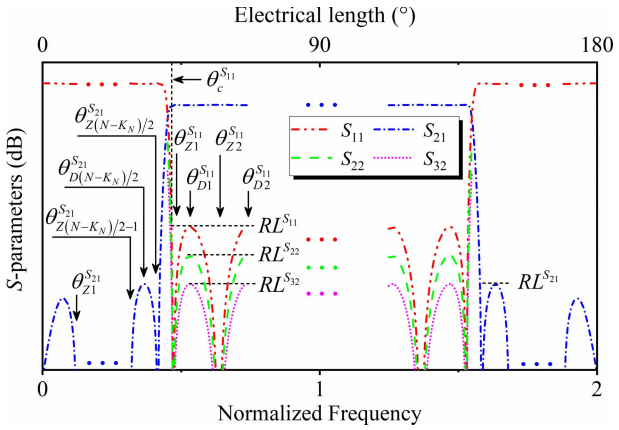

Fig. 3. Schematic of general S-parameters corresponding to the proposed wideband BP PD in Fig. 1.

provide equal-ripple responses of S_{11}, S_{32}, and S_{22} (S_{33}) in the passband but also maintain multi-TZs of S_{21} in the stopband and multi-RZs in the passband. As such, in-band reflection/isolation levels and out-of-band rejection level can be controlled independently.

1) Even-Mode Calculation: Fig. 3 shows the S-parameters in a single period, where there are $(M+1)$ RZs of S_{11} in the passband and $(N-K_N)$ TZs of S_{21} in the stopband.

To realize wideband equal-ripple response of S_{11}, the following equations should be maintained:

$$S_{11}|_{\theta=\theta_{Z1}^{S_{11}}} = S_{11}|_{\theta=\theta_{Z2}^{S_{11}}} = \cdots = S_{11}|_{\theta=\theta_{Z(M+1)}^{S_{11}}} = 0 \quad (11a)$$

$$\left.\frac{\partial S_{11}}{\partial\theta}\right|_{\theta=\theta_{D1}^{S_{11}}} = \left.\frac{\partial S_{11}}{\partial\theta}\right|_{\theta=\theta_{D2}^{S_{11}}} = \cdots = \left.\frac{\partial S_{11}}{\partial\theta}\right|_{\theta=\theta_{DM}^{S_{11}}} = 0 \quad (11b)$$

$$-20\log_{10}|S_{11}| = \mathrm{RL}^{S_{11}} \ @\ \theta_{D1}^{S_{11}}, \theta_{D2}^{S_{11}}, \ldots, \theta_{DM}^{S_{11}} \quad (11c)$$

$$-20\log_{10}|S_{11}| = \mathrm{RL}^{S_{11}} \ @\ \theta_c^{S_{11}} \quad (11d)$$

where $\theta_c^{S_{11}}$ is defined as the electrical length at the lower cutoff frequency; $\mathrm{RL}^{S_{11}}$ is the return loss of S_{11} at $\theta_{D1}^{S_{11}}, \theta_{D2}^{S_{11}}, \ldots$, and $\theta_{DM}^{S_{11}}$, and $\mathrm{RL}^{S_{11}}$ can be selected arbitrarily.

Considering TZs of S_{21} in the stopband under $S_{21}=0$, we have $1/Y_{\text{sine}}=0$ in (1). The number of TZs of S_{21} is only determined by the number of CLSs N. When N is an even integer, there are N TZs; when N is an odd integer, there are $(N-1)$ TZs. Generally, there are $(N-K_N)$ TZs of S_{21} in the stopband. To realize the controllable TZs of S_{21}, the following equations should be maintained:

$$S_{21}|_{\theta=\theta_{Z1}^{S_{21}}} = S_{21}|_{\theta=\theta_{Z2}^{S_{21}}} = \cdots = S_{21}|_{\theta=\theta_{Z(N-K_N)}^{S_{21}}} = 0 \quad (12a)$$

$$\frac{\partial S_{21}}{\partial\theta} = 0 \ @\ \theta_{D(N-K_N)/2}^{S_{21}} \quad (12b)$$

$$-20\log_{10}|S_{21}| = \mathrm{RL}^{S_{21}} \ @\ \theta_{D(N-K_N)/2}^{S_{21}} \quad (12c)$$

where $\mathrm{RL}^{S_{21}}$ is the return loss of S_{21} at $\theta_{D(N-K_N)/2}^{S_{21}}$, and $\mathrm{RL}^{S_{21}}$ can be selected arbitrarily.

To sum up, in the even-mode calculation, there are $(M+3+N/2-K_N/2)$ design equations and $(2M+N)$ variable parameters in (11) and (12), where all the variable parameters are Z_{ei} $(i=1,2,3,\ldots,M+N)$ and Z_{sj} $(j=1,2,3,\ldots,M)$.

2) Odd-Mode Calculation: As can be seen from Fig. 3, there are M equal ripples of S_{22} (S_{33}) and S_{32} in the passband. It is worth mentioning that Γ_e and Γ_o are determined in even- and odd-mode calculation, respectively. Based on (10), if S_{32} is determined, S_{22} (S_{33}) can be fixed accordingly, and vice versa. Therefore, only S_{32} or S_{22} (S_{33}) needs to be determined in odd-mode calculation.

To determine the equal-ripple response of S_{32}, the following equations should be maintained:

$$\left.\frac{\partial S_{32}}{\partial\theta}\right|_{\theta=\theta_{D1}^{S_{11}}} = \left.\frac{\partial S_{32}}{\partial\theta}\right|_{\theta=\theta_{D2}^{S_{11}}} = \cdots = \left.\frac{\partial S_{32}}{\partial\theta}\right|_{\theta=\theta_{DM}^{S_{11}}} = 0 \quad (13a)$$

$$-20\log_{10}|S_{32}| = \mathrm{RL}^{S_{32}} \ @\ \theta_{D1}^{S_{11}}, \theta_{D2}^{S_{11}}, \ldots, \theta_{DM}^{S_{11}} \quad (13b)$$

where $\mathrm{RL}^{S_{32}}$ is the return loss of S_{32} at $\theta_{D1}^{S_{11}}, \theta_{D2}^{S_{11}}, \ldots$, and $\theta_{DM}^{S_{11}}$.

Similarly, the following equations are needed for equal-ripple response of S_{22}

$$\left.\frac{\partial S_{22}}{\partial\theta}\right|_{\theta=\theta_{D1}^{S_{11}}} = \left.\frac{\partial S_{22}}{\partial\theta}\right|_{\theta=\theta_{D2}^{S_{11}}} = \cdots = \left.\frac{\partial S_{22}}{\partial\theta}\right|_{\theta=\theta_{DM}^{S_{11}}} = 0 \quad (14a)$$

$$-20\log_{10}|S_{22}| = \mathrm{RL}^{S_{22}} \ @\ \theta_{D1}^{S_{11}}, \theta_{D2}^{S_{11}}, \ldots, \theta_{DM}^{S_{11}} \quad (14b)$$

where $\mathrm{RL}^{S_{22}}$ is the return loss of S_{22} at $\theta_{D1}^{S_{11}}, \theta_{D2}^{S_{11}}, \ldots$, and $\theta_{DM}^{S_{11}}$.

To sum up, in the odd-mode calculation, there are $(M+K_M)$ design equations and $(2M+2N-K_N)$ variable parameters in (13), where all the variable parameters can be divided into two parts: the odd-mode characteristic impedances Z_{oi} $(i=1,2,3,\ldots,M+N)$ and isolation resistors R_1, $R_2,\ldots,R_{M+N-K_N}$.

B. Proposed Algorithm

To describe the design approach of proposed wideband BP PD clearly, its detailed algorithm is summarized as a flowchart in Fig. 4. In the following, a few critical design steps are further described.

Step 1: Prescribe the bandwidth $\theta_c^{S_{11}}$, return losses of S_{11} and S_{32} (or S_{22}) in the passband: $\mathrm{RL}^{S_{11}}$ and $\mathrm{RL}^{S_{32}}$ ($\mathrm{RL}^{S_{22}}$), out-of-band rejection level of S_{21} in the stopband: $\mathrm{RL}^{S_{21}}$, TZs of S_{21}; $\theta_{Z1}^{S_{21}}$, $\theta_{Z2}^{S_{21}},\ldots$, and $\theta_{Z(N-K_N)}^{S_{21}}$.

Step 2: Based on the above-prescribed specifications, choose suitable section numbers M and N, and then determine the numbers of simultaneous equations and variable parameters of the proposed topology.

Step 3: In even-mode calculation, as M and N are determined, there are $(M+3+N/2-K_N/2)$ simultaneous equations and $(2M+N)$ variable parameters. Because $(2M+N) \geq (M+3+N/2-K_N/2)$ is valid under the condition of $M \geq 2$ and $N \geq 2$, all the characteristic impedances (Z_{ei} and Z_{sj}) can be calculated from (11) to (12) by properly selecting variable parameters. If any characteristic impedances cannot be realized, go back to Step 2, and choose different values of M and N.

Step 4: Similar to Step 3, there are $(M+K_M)$ simultaneous equations and $(2M+2N-K_N)$ variable parameters in odd-mode calculation. Because the number of variable parameters is larger than the number of

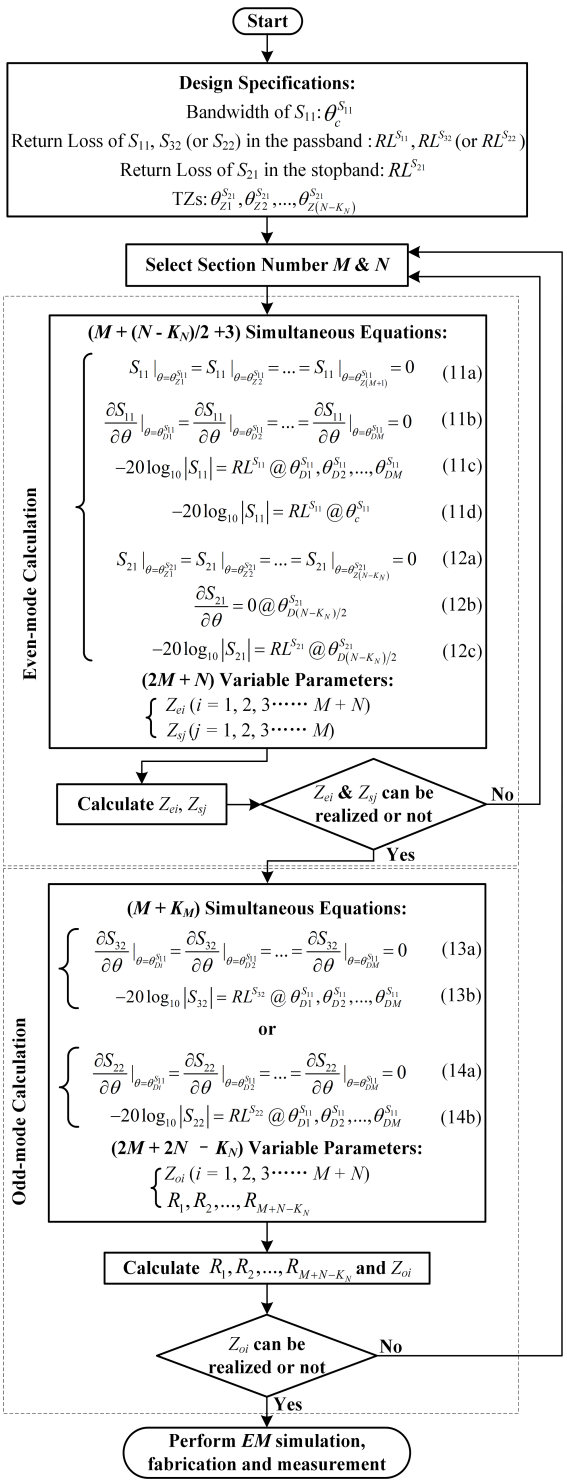

Fig. 4. Design flowchart for the proposed wideband BP PD.

simultaneous equations, $(M + 2N - K_M - K_N)$ variable parameters can be selected arbitrarily to derive a group of unique solutions. Based on the equal-ripple condition of S_{32} (or S_{22}) in (13) [or (14)], all the characteristic impedances (Z_{oi}) and isolation resistors (R_1, R_2, ..., R_{M+N-K_N}) can be calculated by editing and running the MATLAB program. If any odd-mode characteristic impedances cannot be realized, go back to Step 2 and choose different values of M and N.

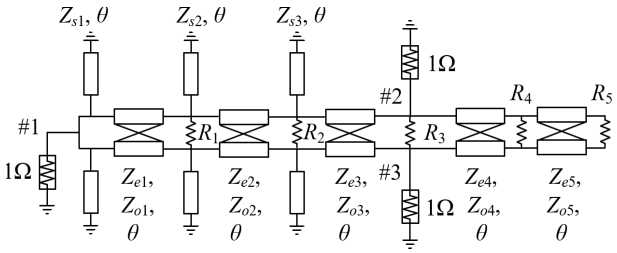

Fig. 5. Proposed wideband BP PD with $M = 3$ and $N = 2$.

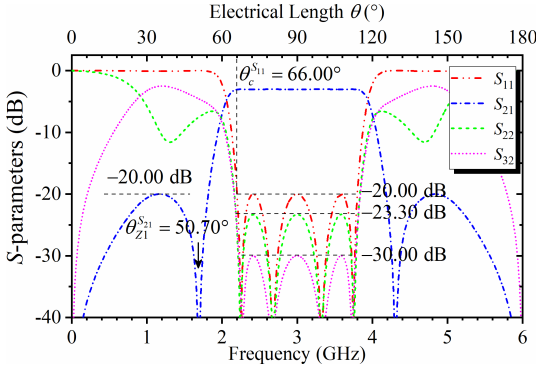

Fig. 6. Circuit simulation results based on Table I for the proposed wideband BP PD (Example A).

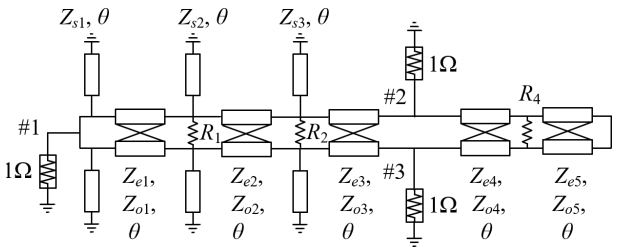

Fig. 7. Optimized wideband BP PD topology with $M = 3$ and $N = 2$.

Step 5: Perform EM simulation and further slightly adjust the physical dimensions toward optimized target if necessary.

IV. Design Examples With Optimization

For the proposed topology in Fig. 1, using the flowchart in Fig. 4, the general response in Fig. 3 will be evidently validated in this section. Several design charts, design examples, and circuit simulation results are given for discussion.

A. $M = 3$ and $N = 2$ (Standard and Optimized Topology)

Fig. 5 shows the proposed wideband BP PD with $M = 3$ and $N = 2$. By substituting $M = 3$ and $N = 2$ into (3) and (8), the ABCD matrices can be obtained directly. Because detailed equations are very complicated and lengthy, they are omitted in this article.

Based on (12a), the electrical length of TZ can be calculated

$$\theta_{TZ1} = \arccos\sqrt{Z_{e4}/(Z_{e4} + Z_{e5})} = \arccos\sqrt{1/1 + k_s} \quad (15)$$

where $k_s = Z_{e5}/Z_{e4}$.

Based on the flowchart in Fig. 4, one design example (Example A) is demonstrated and realized under the conditions of: $\theta_c^{S_{11}} = 66.00°$ at $f_0 = 3$ GHz, $\mathrm{RL}^{S_{11}} = 20$ dB, and $\mathrm{RL}^{S_{32}} = 30$ dB in the passband and $\mathrm{RL}^{S_{21}} = 20$ dB in the

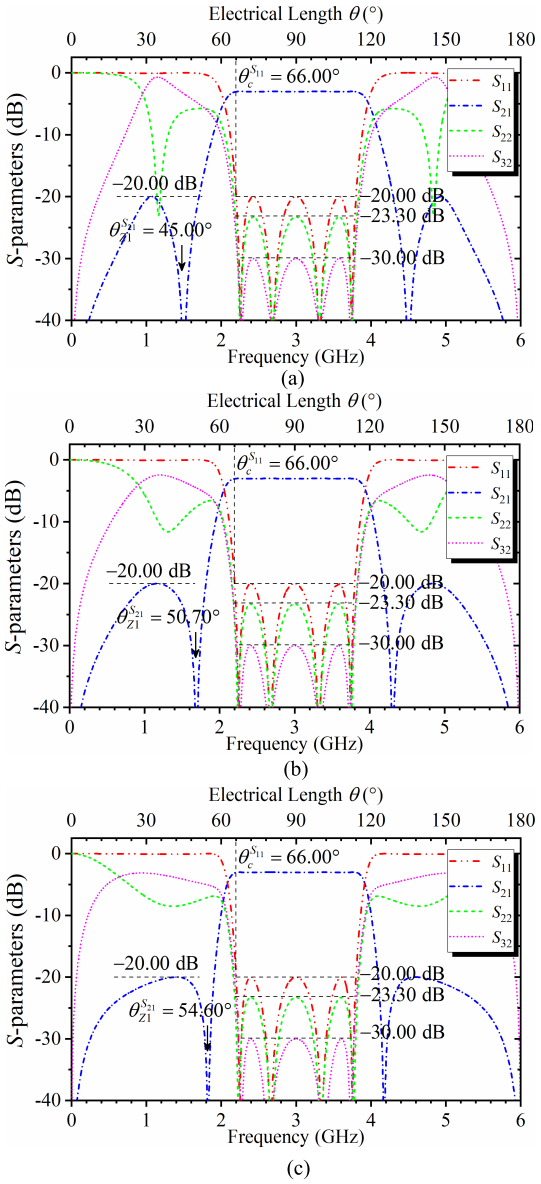

Fig. 8. Circuit simulation results for the optimized wideband BP PDs. (a) Example B. (b) Example C. (c) Example D.

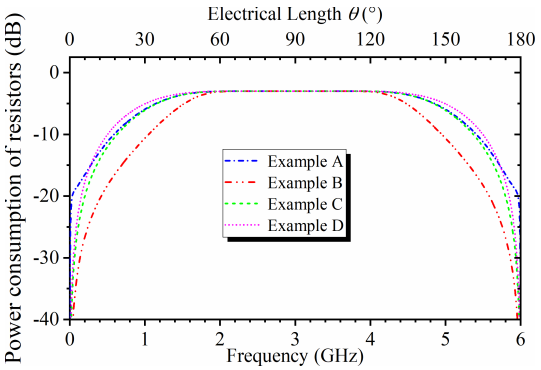

Fig. 9. Frequency versus power consumption of resistors for four wideband BP PDs.

stopband, $\theta_{Z1}^{S_{21}} = 50.70°$. In even-mode calculation, there are seven simultaneous equations ($M + 3 + N/2 - K_N/2 = 7$, where $K_N = 0$) and eight variable parameters (Z_{e1}, Z_{e2}, Z_{e3}, Z_{e4}, Z_{e5}, Z_{s1}, Z_{s2}, and Z_{s3}). When $Z_{s2} = 3.0000\ \Omega$ is given,

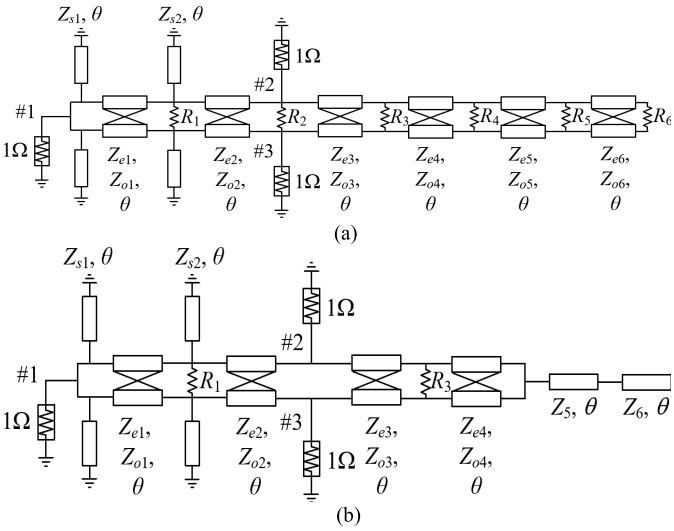

Fig. 10. Proposed wideband BP PD with $M = 2$ and $N = 4$. (a) Standard topology. (b) Optimized topology.

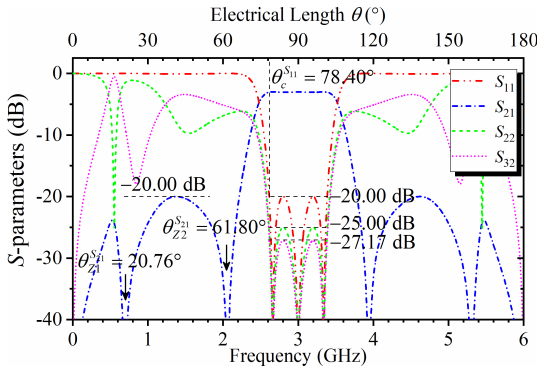

Fig. 11. Circuit simulation results for the optimized wideband BP PD (Example E).

TABLE I

STANDARD TOPOLOGY WITH $M = 3$ AND $N = 2$ (EXAMPLE A)

Characteristic Impedances of CLSs and SCSs (Ω)			Isolation Resistors (Ω)
$Z_{e1} = 2.4090$	$Z_{o1} = 1.4900$	$Z_{s1} = 1.2510$	$R_1 = 11.7362$
$Z_{e2} = 2.3377$	$Z_{o2} = 1.2800$	$Z_{s2} = 3.0000$	$R_2 = 1.5984$
$Z_{e3} = 1.2413$	$Z_{o3} = 1.1300$	$Z_{s3} = 1.1078$	$R_3 = 76.2680$
$Z_{e4} = 1.8942$	$Z_{o4} = 1.7700$		$R_4 = 5.8457$
$Z_{e5} = 2.8413$	$Z_{o5} = 1.7000$		$R_5 = 0.1000$

a group of unique solutions can thus be derived from (11) and (12). In odd-mode calculation, there are four simultaneous equations ($M + K_M = 4$, where $K_M = 1$) and ten variable parameters (Z_{o1}, Z_{o2}, Z_{o3}, Z_{o4}, Z_{o5}, R_1, R_2, R_3, R_4, and R_5). When the coupling strengths of the all CLSs and the resistance of R_5 are determined, a group of unique solutions can be derived from (13). All the calculated parameters are tabulated in Table I. The circuit simulation results are depicted in Fig. 6.

Through carefully analyzing the isolation resistors $R_3 = 76.2680\ \Omega$ and $R_5 = 0.1000\ \Omega$ in Example A, $R_3 \to \infty$ and $R_5 = 0$ can be selected for circuit optimization. Then, the optimized topology is derived as shown in Fig. 7, where two isolation resistors (R_3 and R_5) are omitted.

Three design examples (Example B–D) are studied under the condition of: $\theta_c^{S_{11}} = 66.00°$ at $f_0 = 3$ GHz, $\mathrm{RL}^{S_{11}} = 20$ dB, and $\mathrm{RL}^{S_{32}} = 30$ dB in the passband and

TABLE II
OPTIMIZED TOPOLOGY WITH $M = 3$ AND $N = 2$ (EXAMPLE B)

Characteristic Impedances of CLSs and SCSs (Ω)			Isolation Resistors (Ω)
$Z_{e1} = 2.1642$	$Z_{o1} = 1.5065$	$Z_{s1} = 1.3535$	$R_1 = 2.1106$
$Z_{e2} = 1.5530$	$Z_{o2} = 0.7000$	$Z_{s2} = 3.0000$	$R_2 = 4.4378$
$Z_{e3} = 0.9179$	$Z_{o3} = 0.9160$	$Z_{s3} = 0.4562$	$R_3 = \infty$
$Z_{e4} = 1.7257$	$Z_{o4} = 1.7240$		$R_4 = 3.6777$
$Z_{e5} = 1.7257$	$Z_{o5} = 0.9200$		$R_5 = 0$

TABLE III
OPTIMIZED TOPOLOGY WITH $M = 3$ AND $N = 2$ (EXAMPLE C)

Characteristic Impedances of CLSs and SCSs (Ω)			Isolation Resistors (Ω)
$Z_{e1} = 2.4090$	$Z_{o1} = 1.7106$	$Z_{s1} = 1.2510$	$R_1 = 12.3335$
$Z_{e2} = 2.3377$	$Z_{o2} = 1.3200$	$Z_{s2} = 3.0000$	$R_2 = 1.5779$
$Z_{e3} = 1.2413$	$Z_{o3} = 1.1000$	$Z_{s3} = 1.1078$	$R_3 = \infty$
$Z_{e4} = 1.8942$	$Z_{o4} = 1.7600$		$R_4 = 5.6028$
$Z_{e5} = 2.8413$	$Z_{o5} = 1.7000$		$R_5 = 0$

TABLE IV
OPTIMIZED TOPOLOGY WITH $M = 3$ AND $N = 2$ (EXAMPLE D)

Characteristic Impedances of CLSs and SCSs (Ω)			Isolation Resistors (Ω)
$Z_{e1} = 2.6571$	$Z_{o1} = 0.7027$	$Z_{s1} = 1.1720$	$R_1 = 43.8318$
$Z_{e2} = 3.7165$	$Z_{o2} = 1.2000$	$Z_{s2} = 3.0000$	$R_2 = 2.1184$
$Z_{e3} = 1.7892$	$Z_{o3} = 1.3000$	$Z_{s3} = 5.2219$	$R_3 = \infty$
$Z_{e4} = 2.1604$	$Z_{o4} = 1.8800$		$R_4 = 7.3495$
$Z_{e5} = 4.3208$	$Z_{o5} = 2.0000$		$R_5 = 0$

$\mathrm{RL}^{S_{21}} = 20$ dB in the stopband. Different TZs of S_{21} need to be selected in these three examples, where $\theta_{Z1}^{S_{21}} = 45.00°$ in Example B, $\theta_{Z1}^{S_{21}} = 50.70°$ in Example C, and $\theta_{Z1}^{S_{21}} = 54.60°$ in Example D.

In even-mode calculation, under the only degree of freedom in $Z_{s2} = 3.0000\ \Omega$, a group of unique solutions can be derived from (11) and (12). In odd-mode calculation, there are 6 degrees of freedom. Because $R_3 \to \infty$ and $R_5 = 0\ \Omega$ are known, the left 4 degrees of freedom are consumed by Z_{o2}–Z_{o5}. Then, a group of unique solutions can be derived from (13). For three design examples, the detailed calculation parameters are tabulated in Tables II–IV, respectively. Their circuit simulation results are depicted in Fig. 8(a)–(c).

The power consumption of the resistors is also considered here, and its values are calculated as depicted in Fig. 9 from $|S_{12}|^2 + |S_{22}|^2 + |S_{32}|^2 + |S_R|^2 = 1$. Under the same TZs, the power consumption of resistors between Example A and C is almost the same. Comparing three examples (Example B–D), sharp roll-off rate can be enhanced as the TZs are shifted to the center frequency; meanwhile, the bandwidth of power consumption becomes wider.

B. $M = 2$ and $N = 4$ (Standard and Optimized Topology)

Similarly, the proposed topology can also be designed with different values of M and N. Fig. 10 shows the standard topology and its optimized case with $M = 2$ and $N = 4$. Compared with standard topology, $R_2 \to \infty$ and $R_4 = 0\ \Omega$ are preferred for optimization. Naturally, $R_5 = R_6 = 0$, then the fifth and sixth CLSs are two cascaded transmission lines.

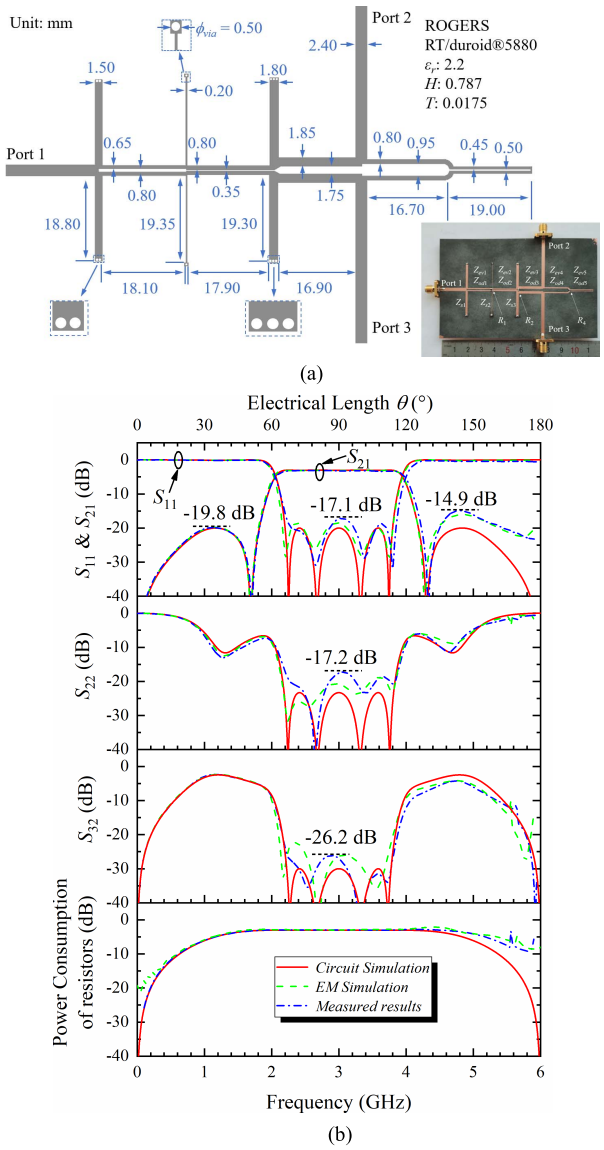

Fig. 12. Experimental circuit of the proposed wideband BP PD (Example C). (a) Layout and photograph of the circuit. (b) Circuit simulation, EM simulation, and measured results.

TABLE V
OPTIMIZED TOPOLOGY WITH $M = 2$ AND $N = 4$ (EXAMPLE E)

Characteristic Impedances of CLSs and SCSs (Ω)			Isolation Resistors (Ω)
$Z_{e1} = 2.3303$	$Z_{o1} = 1.9000$	$Z_{s1} = 0.5611$	$R_1 = 1.4799$
$Z_{e2} = 1.6478$	$Z_{o2} = 1.6200$	$Z_{s2} = 0.9725$	$R_2 = \infty$
$Z_{e3} = 1.0678$	$Z_{o3} = 1.0400$		$R_3 = 1.6293$
$Z_{e4} = 1.7085$	$Z_{o4} = 1.4000$		$R_4 = 0$
$Z_5 = 1.7085$			$R_5 = 0$
$Z_6 = 0.5339$			$R_6 = 0$

Instead of the detailed design equations and discussions, only optimized topology (Example E) is given herein as an example.

The design parameters of Example E under the condition of: $\theta_c^{S_{11}} = 78.40°$ at $f_0 = 3$ GHz, $\mathrm{RL}^{S_{11}} = 20$ dB, and $\mathrm{RL}^{S_{22}} = 25$ dB in the passband and $\mathrm{RL}^{S_{21}} = 20$ dB in the stopband, $\theta_{Z1}^{S_{21}} = 20.76°$ and $\theta_{Z2}^{S_{21}} = 61.80°$. The detailed calculation parameters are tabulated in Table V, and the circuit simulation results are shown in Fig. 11.

TABLE VI
COMPARISON OF SEVERAL RECENT WIDEBAND BP PDS [17]–[36]

Ref.	f_0 (GHz) / *FBW* (%)	No. of RZs / TZs ($0 \sim 2f_0$)	Ripple levels of *S*-parameters (dB)			Equal-ripple responses of S_{22} / S_{32} with controllable ripple levels	TZs and out-of-band rejection can be designed independently	Size (λ_g*λ_g)
			Out-of-band rejection (dB)	Reflection S_{11} / S_{22} (dB)	Isolation S_{32} (dB)			
[17]	7.0 / 107.1	2 / None	-	-10 / -10	-8	No / No	No	-
[18]	6.85 / 100.7	4 / 1	-17	-10 / -10	-10	No / No	No	-
[19]	7.0 / 82.9	3 / None	-	- / -15	-	No / No	No	0.36*0.27
[20]	6.0 / 110	4 / None	-	-11.2 / -11.5	-15	No / No	No	-
[21]	3.0 / 90	3 / 3	-	-15 / -	-17	No / No	No	0.80*0.50
[22]	2.05 / 62.5	3 / 2	-15.8	-10.14 / -	-	No / No	No	-
[23]	7 / 94	4 / 2	-	-10 / -	-	No / No	No	>0.50*0.50
[24]	3.01 / 70	2 / 2	-13	-16 / -	-16.7	No / No	No	0.40*0.29
[25]	2.0 / 104.5	3 / 1	-17.2	-15 / -	-18.1	No / No	No	0.2*0.15
[26]	2.3 / 31	3 / 2	-	- / -	-17	No / No	No	0.64*0.32
[27]	2.0 / 62	1 / None	-	-15 / -	-15	No / No	No	0.55*0.36
[28]	2.02 / 49.5	3 / 2	-40	-15 / -15	-22	No / No	No	0.23*0.22
[29]	3.0 / 107.3	4 / None	-	-17.8 / -	-19.8	No / No	No	1.68*0.57
[30]	2.5 / 78	4 / 2	-	- / -	-17.5	No / No	No	0.74*0.31
[31]	3.0 / 66	4 / None	-	-21.1 / -19.2	-18.5	No / No	No	0.56*0.18
[32]	7.0 / 107.1	2 / None	-	-13 / -13	-15	No / No	No	-
[33]	1.0 / 50	3 / 2	-10	- / -	-12	No / No	No	0.16*0.55
[34]	1.5 / 56.5	2 / 2	-15	-10 / -13	-15	No / No	No	0.32*0.32
[35]	4.0 / 86.4	2 / 2	-	-12 / -	-17	No / No	No	-
[36]	2.1 / 47.6	2 / 2	-	-16.1 / -17.6	-20.2	No / No	No	0.63*0.33
This work	**3.0 / 53**	**4 / 2**	**-19.8/-14.9**	**-17.1 / -17.2**	**-26.2**	**Yes / Yes**	**Yes**	**1.30*0.56**
	3.0 / 26	**3 / 4**	**-20.8/-15.3**	**-23.1 / -21.6**	**-21.6**	**Yes / Yes**	**Yes**	**1.54*0.56**

V. EXPERIMENTS AND DISCUSSION

In the experiment, two prototype circuits (Examples C and E) are selected for fabrication on Rogers RT/5880 substrate. For the first experimental circuit, Fig. 12(a) shows the layout and photograph of Example C. The detailed design parameters are listed in Table III, where the resistances of resistors are $R_1 = 619\ \Omega$, $R_2 = 75\ \Omega$, and $R_4 = 280\ \Omega$. Fig. 12(b) shows the results from circuit simulation, EM simulation (Sonnet), and measurements. Similarly, the layout circuit, photograph, simulated, and measured results of the second experimental circuit (Example E) are shown in Fig. 13(a) and (b), respectively, where the resistances of resistors are $R_1 = 75\ \Omega$ and $R_3 = 82\ \Omega$.

The even- and odd-modes propagating along the CLSs have different phase velocities in microstrip line structure, where $v_{ev} \neq v_{od}$. When the coupling between these two modes is very weak, the maximum coupling strengths in the first and second experimental circuits are -11.11 and -19.86 dB, respectively. $v_{ev} \approx v_{od}$ can be assumed in two experimental circuits. Furthermore, parasitic effect around via-holes and multi-transmission line junctions will affect the concerned performances, especially at high frequencies. Therefore, for both the sets of experiments, the simulated and measured results are matched very well until 4.5 GHz.

Finally, a comparison among several other reported works [17]–[36] is listed in Table VI. From Table VI, the following improvements can be achieved as summarized.

1) By selecting different M and N, the number of RZs and TZs can be designed arbitrarily. In the experiment, four RZs and two TZs are realized in the first experimental circuit; three RZs and four TZs are realized in the second experimental circuit.
2) Equal-ripple responses of S_{11}, S_{22}, S_{33}, and S_{32} can be maintained, and their ripple levels can also be designed at the same time.

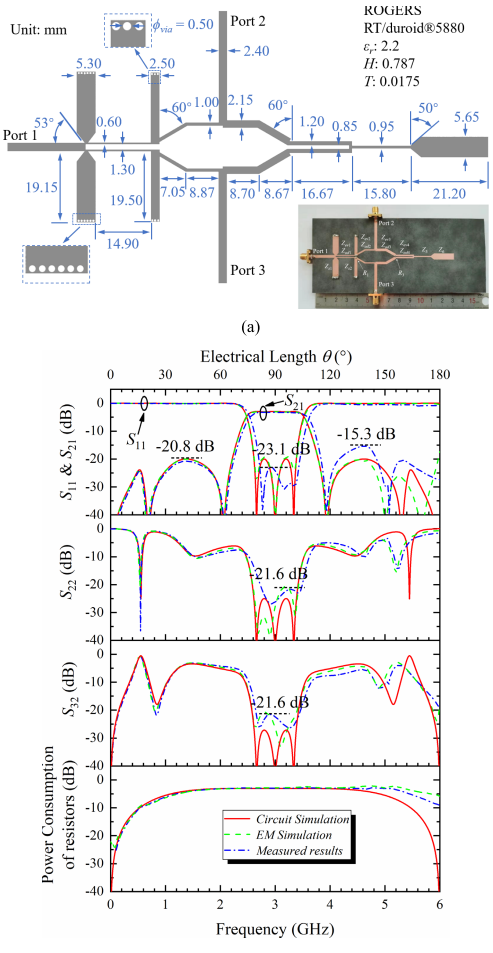

Fig. 13. Experimental circuit of the proposed wideband BP PD (Example E). (a) Layout and photograph of the circuit. (b) Circuit simulation, EM simulation, and measured results.

3) Furthermore, even though the bandwidth is determined, TZs and out-of-band rejection level can be designed independently.

VI. Conclusion

In this article, a novel class of wideband bandpass PDs with out-of-band multi-TZs have been presented and designed. A set of general simultaneous equations for characteristic impedances, coupling strengths, and isolation resistors have been systematically summarized through even- and odd-mode analyses. Based on the proposed algorithm, a group of unique solutions could be derived, and controllable equal-ripple responses of S_{11}, S_{21} (S_{31}), S_{22} (S_{33}), and S_{32} could be realized in the passband. The out-of-band rejection level and TZs could be designed independently. For further optimization, several isolation resistors have been omitted under the same performance. For verification, two experimental circuits have been fabricated, and the measured frequency responses have verified well the proposed design theory.

References

[1] E. J. Wilkinson, "An N-way hybrid power divider," *IRE Trans. Microw. Theory Techn.*, vol. MTT-8, no. 1, pp. 116–118, Jan. 1960.

[2] Y. C. Li, Q. Xue, and X. Y. Zhang, "Single and dual-band power dividers integrated with bandpass filters," *IEEE Trans. Microw. Theory Techn.*, vol. 61, no. 1, pp. 69–76, Jan. 2013.

[3] X.-L. Zhao, L. Gao, X. Y. Zhang, and J.-X. Xu, "Novel filtering power divider with wide stopband using discriminating coupling," *IEEE Microw. Wireless Compon. Lett.*, vol. 26, no. 8, pp. 580–582, Aug. 2016.

[4] C.-J. Chen and Z.-C. Ho, "Design equations for a coupled-line type filtering power divider," *IEEE Microw. Wireless Compon. Lett.*, vol. 27, no. 3, pp. 257–259, Mar. 2017.

[5] Y. L. Wu, Z. Zhuang, G. Y. Yan, Y. A. Liu, and Z. Ghassemlooy, "Generalized dual-band unequal filtering power divider with independently controllable bandwidth," *IEEE Trans. Microw. Theory Techn.*, vol. 65, no. 10, pp. 3838–3848, Oct. 2017.

[6] G. Shen, W. Che, Q. Xue, and W. Feng, "Novel design of miniaturized filtering power dividers using dual-composite right-/left-handed resonators," *IEEE Trans. Microw. Theory Techn.*, vol. 66, no. 12, pp. 5260–5271, Dec. 2018.

[7] B. Lee, S. Nam, and J. Lee, "Filtering power divider with reflectionless response and wide isolation at output ports," *IEEE Trans. Microw. Theory Techn.*, vol. 67, no. 7, pp. 2684–2692, Jul. 2019.

[8] G. Shen, W. Che, W. Feng, and Q. Xue, "High-isolation topology for filtering power dividers based on complex isolation impedance and surface wave suppression," *IEEE Trans. Microw. Theory Techn.*, vol. 69, no. 1, pp. 43–53, Jan. 2021.

[9] U. Rosenberg, M. Salehi, J. Bornemann, and E. Mehrshahi, "A novel frequency-selective power combiner/divider in single-layer substrate integrated waveguide technology," *IEEE Microw. Wireless Compon. Lett.*, vol. 23, no. 8, pp. 406–408, Aug. 2013.

[10] X. Y. Zhang, K.-X. Wang, and B.-J. Hu, "Compact filtering power divider with enhanced second-harmonic suppression," *IEEE Microw. Wireless Compon. Lett.*, vol. 23, no. 9, pp. 483–485, Sep. 2013.

[11] C.-F. Chen and C.-Y. Lin, "Compact microstrip filtering power dividers with good in-band isolation performance," *IEEE Microw. Wireless Compon. Lett.*, vol. 24, no. 1, pp. 17–19, Jan. 2014.

[12] W.-M. Chau, K.-W. Hsu, and W.-H. Tu, "Filter-based Wilkinson power divider," *IEEE Microw. Wireless Compon. Lett.*, vol. 24, no. 4, pp. 239–241, Apr. 2014.

[13] G. Zhang, J. Wang, L. Zhu, and W. Wu, "Dual-band filtering power divider with high selectivity and good isolation," *IEEE Microw. Wireless Compon. Lett.*, vol. 26, no. 10, pp. 774–776, Oct. 2016.

[14] G. Zhang, X. D. Wang, J.-S. Hong, and J. Q. Yang, "A high-performance dual-mode filtering power divider with simple layout," *IEEE Microw. Wireless Compon. Lett.*, vol. 28, no. 2, pp. 120–122, Feb. 2018.

[15] P. Wen *et al.*, "Dual-band filtering power divider using dual-resonance resonators with ultrawide stopband and good isolation," *IEEE Microw. Wireless Compon. Lett.*, vol. 29, no. 2, pp. 101–103, Feb. 2019.

[16] D. Psychogiou, R. Gómez-García, A. C. Guyette, and D. Peroulis, "Reconfigurable single/multi-band filtering power divider based on quasi-bandpass sections," *IEEE Microw. Wireless Compon. Lett.*, vol. 26, no. 9, pp. 684–686, Sep. 2016.

[17] M. E. Bialkowski and A. M. Abbosh, "Design of a compact UWB Out-of-Phase power divider," *IEEE Microw. Wireless Compon. Lett.*, vol. 17, no. 4, pp. 289–291, Apr. 2007.

[18] K. Song and Q. Xue, "Novel ultra-wideband (UWB) multilayer slotline power divider with bandpass response," *IEEE Microw. Compon. Lett.*, vol. 20, no. 1, pp. 13–15, Jan. 2010.

[19] K. Song, Y. Zhu, Q. Duan, M. Fan, and Y. Fan, "Extremely compact ultra-wideband power divider using hybrid slotline/microstrip-line transition," *Electron. Lett.*, vol. 51, no. 24, pp. 2014–2015, Nov. 2015.

[20] H. Zhu, Z. Cheng, and Y. J. Guo, "Design of wideband in-phase and out-of-phase power dividers using microstrip-to-slotline transitions and slotline resonators," *IEEE Trans. Microw. Theory Techn.*, vol. 67, no. 4, pp. 1412–1424, Apr. 2019.

[21] L. Jiao, Y. Wu, Y. Liu, Q. Xue, and Z. Ghassemlooy, "Wideband filtering power divider with embedded transversal signal-interference sections," *IEEE Microw. Wireless Compon. Lett.*, vol. 27, no. 12, pp. 1068–1070, Dec. 2017.

[22] S. S. Gao, S. Sun, and S. Xiao, "A novel wideband bandpass power divider with harmonic-suppressed ring resonator," *IEEE Microw. Wireless Compon. Lett.*, vol. 23, no. 3, pp. 119–121, Mar. 2013.

[23] S. W. Wong and L. Zhu, "Ultra-wideband power divider with good in-band splitting and isolation performances," *IEEE Microw. Wireless Compon. Lett.*, vol. 18, no. 8, pp. 518–520, Aug. 2008.

[24] B. Zhang and Y. Liu, "Wideband filtering power divider with high selectivity," *Electron. Lett*, vol. 51, no. 23, pp. 1950–1952, Nov. 2015.

[25] C.-W. Tang and J.-T. Chen, "A design of 3-dB wideband microstrip power divider with an ultra-wide isolated frequency band," *IEEE Trans. Microw. Theory Techn.*, vol. 64, no. 6, pp. 1806–1811, Jun. 2016.

[26] Y. Deng, J. Wang, and J.-L. Li, "Design of compact wideband filtering power divider with extended isolation and rejection bandwidth," *Electron. Lett.*, vol. 52, no. 16, pp. 1387–1389, Aug. 2016.

[27] M. A. Maktoomi, M. S. Hashmi, and F. M. Ghannouchi, "Theory and design of a novel wideband dc isolated Wilkinson power divider," *IEEE Microw. Wireless Compon. Lett.*, vol. 26, no. 8, pp. 586–588, Aug. 2016.

[28] M.-T. Chen and C.-W. Tang, "Design of the filtering power divider with a wide passband and stopband," *IEEE Microw. Wireless Compon. Lett.*, vol. 28, no. 7, pp. 570–572, Jul. 2018.

[29] X. Wang, Z. Ma, T. Xie, M. Ohira, C.-P. Chen, and G. Lu, "Synthesis theory of ultra-wideband bandpass transformer and its Wilkinson power divider application with perfect in-band reflection/isolation," *IEEE Trans. Microw. Theory Techn.*, vol. 67, no. 8, pp. 3377–3390, Aug. 2019.

[30] Y. Liu, L. Zhu, and S. Sun, "Proposal and design of a power divider with wideband power division and port-to-port isolation: A new topology," *IEEE Trans. Microw. Theory Techn.*, vol. 68, no. 4, pp. 1431–1438, Apr. 2020.

[31] C. Bao, X. Wang, Z. Ma, C.-P. Chen, and G. Lu, "An optimization algorithm in ultrawideband bandpass Wilkinson power divider for controllable equal-ripple level," *IEEE Microw. Wireless Compon. Lett.*, vol. 30, no. 9, pp. 861–864, Sep. 2020.

[32] A. M. Abbosh, "Design of ultra-wideband three-way arbitrary power dividers," *IEEE Trans. Microw. Theory Techn.*, vol. 56, no. 1, pp. 194–201, Jan. 2008.

[33] K. Song, Y. Mo, and Y. Fan, "Wideband four-way filtering-response power divider with improved output isolation based on coupled lines," *IEEE Microw. Wireless Compon. Lett.*, vol. 24, no. 10, pp. 674–676, Oct. 2014.

[34] H. Zhu, A. M. Abbosh, and L. Guo, "Wideband four-way filtering power divider with sharp selectivity and wide stopband using looped coupled-line structures," *IEEE Microw. Wireless Compon. Lett.*, vol. 26, no. 6, pp. 413–415, Jun. 2016.

[35] X. Zhao, K. Song, Y. Zhu, and Y. Fan, "Wideband four-way filtering power divider with isolation performance using three parallel-coupled lines," *IEEE Microw. Wireless Compon. Lett.*, vol. 27, no. 9, pp. 800–802, Sep. 2017.

[36] G. Zhang, Z. Qian, J. Yang, and J.-S. Hong, "Wideband four-way filtering power divider with sharp selectivity and high isolation using coshared multi-mode resonators," *IEEE Microw. Wireless Compon. Lett.*, vol. 29, no. 10, pp. 641–644, Oct. 2019.

Nan Zhang was born in Changchun, China, in 1996. He received the B.S. degree from the College of Electronic Science and Engineering, Jilin University, Changchun, China, in 2017, where he is currently pursuing the Ph.D. degree.

His current research interests include the analysis and design of microwave passive components and microwave sensors.

Xiaolong Wang (Member, IEEE) received the B.S. degree in communication engineering from Jilin University, Changchun, China, in 2005, the M.S. degree from Changchun University of Science and Technology, Changchun, in 2008, and the Ph.D. degree from University of Toyama, Toyama, Japan, in 2012.

From November 2012 to June 2013, he was a Post-Doctoral Research Associate with the Art, Science and Technology Center for Cooperative Research, Kyushu University, Fukuoka, Japan. From July 2013 to December 2015, he was a Researcher with the Plasma Research Center, University of Tsukuba, Tsukuba, Japan. Since January 2016, he has been an Assistant Professor with the Department of Electronic Engineering, Saitama University, Japan. Now, he is a Professor with the college of electronic science and engineering, Jilin University. His research interests include microwave/millimeter-wave system design, passive component design, and optimization techniques.

Dr. Wang is a member of the Institute of Electronics, Information and Communication Engineers (IEICE), Japan. He was the recipient of the IEEE MTT-S Japan Chapter Young Engineer Award in 2013.

Lei Zhu (Fellow, IEEE) received the B.Eng. and M.Eng. degrees in radio engineering from Nanjing Institute of Technology (now Southeast University), Nanjing, China, in 1985 and 1988, respectively, and the Ph.D. degree in electronic engineering from the University of Electro-Communications, Tokyo, Japan, in 1993.

From 1993 to 1996, he was a Research Engineer with Matsushita–Kotobuki Electronics Industries Ltd., Tokyo, Japan. From 1996 to 2000, he was a Research Fellow with the École Polytechnique de Montreal, Montreal, QC, Canada. From 2000 to 2013, he was an Associate Professor with the School of Electrical and Electronic Engineering, Nanyang Technological University, Singapore. He joined the Faculty of Science and Technology, University of Macau, Macau, China, as a Full Professor in August 2013, where he has been a Distinguished Professor since December 2016. From August 2014 to August 2017, he served as the Head of the Department of Electrical and Computer Engineering, University of Macau, Macau, China. So far, he has authored or coauthored more than 685 articles in international journals and conference proceedings. His articles have been cited more than 12 000 times with the H-index of 55 (source: Scopus). His research interests include microwave circuits, antennas, periodic structures, and computational electromagnetics.

Dr. Zhu served as the member for IEEE MTT-S Fellow Evaluation Committee from 2013 to 2015, and IEEE AP-S Fellows Committee from 2015 to 2017. He was the recipient of the 1993 Achievement Award in Science and Technology (first prize) from the National Education Committee of China, the 1996 Silver Award of Excellent Invention from Matsushita–Kotobuki Electronics Industries Ltd., the 1997 Asia–Pacific Microwave Prize Award, the 2020 FST Research Excellence Award from the University of Macau, and the 2020 Macao Natural Science Award (second prize) from the Science and Technology Development Fund (FDCT), Macau. He served as a General Chair for the 2008 IEEE MTT-S International Microwave Workshop Series on the Art of Miniaturizing RF and Microwave Passive Components, Chengdu, China, and a Technical Program Committee Co-Chair of the 2009 Asia–Pacific Microwave Conference, Singapore. He was the Associate Editor of the IEEE TRANSACTIONS ON MICROWAVE THEORY AND TECHNIQUES from 2010 to 2013 and IEEE Microwave and Wireless Components Letters from 2006 to 2012.

Geyu Lu received the B.Sc. degree in electronic sciences and the M.S. degree from Jilin University, Changchun, China, in 1985 and 1988, respectively, and the Dr.Eng. degree from Kyushu University, Fukuoka, Japan, in 1998.

Now he is a Professor with Jilin University. His current research interests include the development of chemical sensors and the application of function materials.